JOURNAL OF Materials CHEMISTRY

New oxygen-deficient perovskite series, $Ca_2Mn_{2-x}Nb_xO_\gamma$: $0 < x < 1.2$

Angela Kruth,[a]† Ulrich Guth[b] and Anthony R. West[a]†

[a]*Department of Chemistry, University of Aberdeen, Meston Walk, Aberdeen, UK*
[b]*Institute of Chemistry and Biochemistry, University of Greifswald, Soldtmannstraße, Greifswald, Germany*

Received 22nd March 1999, Accepted 29th April 1999

An extensive range of orthorhombic perovskites with the $GdFeO_3$ structure, variable B-cation content and variable oxygen content form according to the formula $Ca_2Mn_{2-x}Nb_xO_\gamma$: $0 < x < 1.2$. A second, closely-related, oxygen-deficient solid solution with a simple cubic perovskite structure forms over the range $0.3 < x < 0.8$. Oxygen contents range from $5.0 < \gamma < 6.0$ for $x = 0$ to $5.8 < \gamma < 6.0$ for $x = 1.2$ and are obtained by post-reaction heat treatment, either in air at different temperatures or in H_2–N_2. The orthorhombic solid solutions are either oxygen-stoichiometric or lightly reduced and transform to the cubic structure on more extensive reduction. A phase diagram is presented showing the equilibrium γ values in air over the temperature range 1000–1350 °C. The variable composition of the solid solutions is accommodated by vacancies in up to 20% of the oxygen positions and variations in the oxidation state of Mn, between +2 and +4.

Introduction

In perovskites, variable oxygen content is one of the most important parameters determining attractive physical properties such as GMR (giant magnetoresistance), oxide ion conduction, superconductivity and catalytic activity. Some oxygen-deficient perovskites are well-characterised, *e.g.* $AXO_{3-\delta}$: A = Ca, Sr; X = Fe, Mn, Co;[1–8] oxygen non-stoichiometry results in ordered structures which can be described as superlattice repeats of the parent perovskites. Oxygen content and transition metal oxidation states can be controlled, not only by post-reaction heat treatment at different temperatures or oxygen partial pressures, but also by aliovalent doping and associated charge compensation.

We are interested in materials derived from $CaMnO_3$ for possible catalyst and sensor applications.[9] Previously,[10] we characterised a new oxygen-deficient perovskite, Ca_2MnNbO_γ on the binary join $CaMnO_3$–$Ca_2Nb_2O_7$. It has an orthorhombic $GdFeO_3$ structure and γ varying from 5.86 to 6.00. In oxygen-deficient compositions, Mn occurs in a mixed valence state (2+, 3+). It shows p-type semiconducting properties, exhibits Curie–Weiss paramagnetism at high temperatures and provides another example of spin-glass like behaviour at low temperatures, as seen in the related phases A_2FeXO_6: A = Ca, Sr, Ba; X = Nb, Ta, Sb.[11–15]

This paper characterises an extensive range of new solid solutions of general formula $Ca_2Mn_{2-x}Nb_xO_\gamma$ with $0 \leqslant x \leqslant 1.2$, which includes the previously reported phase Ca_2MnNbO_γ with $x = 1.0$. The compositional variables of the solid solutions are Nb content, oxygen content and associated manganese valence.

Experimental

Starting materials, $CaCO_3$ (99% AnalaR) and Nb_2O_5 (99.9% Aldrich), were dried at 200 and 600 °C, respectively. MnO_2 (99% Aldrich) was used directly from the bottle since a TG study had confirmed its stoichiometry.[9] Appropriate quantities of the metal oxides and carbonate giving 5 g total weight were mixed in acetone for at least 10 min, dried and heated in Pt boats at 900 °C overnight and then at 1200 °C for 20 h. Additional re-heating was carried out from 1250 to 1350 °C in steps of 50 °C for periods of 20 h at each temperature, with regrinding between each heating period. Products were finally fired at 1400 °C for 3 days.

Phase identity and purity were determined by powder X-ray diffraction using a Hägg–Guinier camera. For more accurate work, including indexing and lattice parameter refinement, a Philips Diffractometer PW1710 and STOE STADI P software were used. KCl was added as internal standard and data were collected in the range 20–80° 2θ using CuKα_1 radiation, λ = 1.54056 Å.

Thermogravimetric studies were carried out in a Stanton Redcroft TG-DTA 1500 combined system. Oxygen contents were determined from the weight loss during complete reduction of Mn^{3+}/Mn^{4+} to Mn^{2+} in 10% H_2–90% N_2. The temperature was increased at 10 °C min^{-1} to constant weight when it was assumed that all Mn was reduced to an oxidation state of +2. From the total weight loss, the oxygen content and therefore the initial Mn oxidation state was calculated.

To attempt to modify the oxygen stoichiometry γ, post-reaction treatments in H_2–N_2, air and high pressure O_2 were carried out. In high pressure O_2, samples were heated at 5 °C min^{-1} to 800 °C, held for 16 h and cooled at 2 °C min^{-1}. The maximum pressure was *ca.* 100 atm at 800 °C. Heat treatments in air and 10% H_2–90% N_2 were carried out in the TG instrument which allowed the weight losses to be determined *in situ*. In air, samples were heated to 1350 °C at 10 °C min^{-1}, held for 5 min and cooled at the same rate; in H_2–N_2, samples of known oxygen content were heated to temperatures between 500 and 1200 °C at 10 °C min^{-1}, held for 1 min and cooled at 20 °C min^{-1}.

Results

Solid solution formation: cation compositions

A range of samples with compositions on the join $CaMnO_3$–$Ca_2Nb_2O_7$ were prepared in 5–10 g quantities. They were given a final heating in air at 1400 °C and air-cooled to room temperature over *ca.* 30–60 s by removing from the furnace and placing on a metal plate. XRD patterns indicated the presence of an extensive range of solid solutions, $Ca_2Mn_{2-x}Nb_xO_\gamma$: $0 < x < 1.2$. The patterns were similar to those of $CaMnO_3$[16] and Ca_2MnNbO_6[10] and indicated an orthorhombic unit cell in which the orthorhombic splitting increased with x. From these XRD data, the complete range

†Current address: Department of Engineering Materials, University of Sheffield, Mappin St, Sheffield, UK.

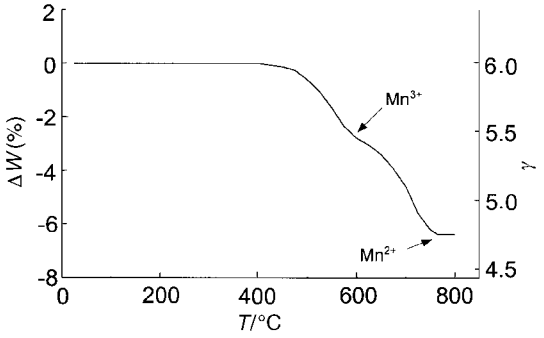

Fig. 1 Weight loss of $Ca_2Mn_{1.5}Nb_{0.5}O_{5.96(3)}$ during reduction in 10% H_2–90% N_2.

of $Ca_2Mn_{2-x}Nb_xO_\gamma$ solid solutions appear to have a $GdFeO_3$-related structure similar to that reported earlier for $x=1.0$, $\gamma=6.0$, *i.e.* Ca_2MnNbO_6. The solid solution limit at 1400 °C is $x\approx1.2$; for $x>1.2$, $Ca_2Nb_2O_7$[17] was observed as a second phase.

Oxygen contents and polymorphism

Oxygen contents γ were obtained by H_2-reduction TG. A typical example is shown in Fig. 1 for $x=0.50$. Weight loss commenced at *ca.* 400 °C and was complete by *ca.* 750 °C. Similar behaviour was observed with other compositions although the temperatures over which weight loss occurred generally increased with x, from 400–750 °C for $x=0$ to 600–1050 °C for $x=1.2$. In order to analyse the TG data, the initial assumption was made that the final products of reduction contained Mn in the +2 state. The results of all subsequent experiments supported the correctness of this assumption. In order to investigate whether reduction of Ca^{2+} or Nb^{5+} occurred, $Ca_2Nb_2O_7$ was heated in H_2–N_2. No weight changes were observed up to 1350 °C and, from XRD, the initial and final compositions were identical. Therefore, it was concluded that only Mn was reduced in $Ca_2Mn_{2-x}Nb_xO_\gamma$ compositions. The products of reduction were also not known initially, but this did not affect the calculation of oxygen contents γ. For most compositions x, the γ values for as-prepared samples were close to 6.00 (Fig. 2), as expected for fully oxidised samples with the $GdFeO_3$ structure. For two compositions however, $x=0$ and $x=1.0$, the γ values were much less, *ca.* 5.65 and *ca.* 5.87, respectively. In order to investigate the maximum γ values that could be readily attained, a selection of samples were treated in O_2 at high pressure and temperature. For all samples, including $x=0$ and $x=1.0$, the resulting γ values obtained were 6.00 within errors (Fig. 2).

The TG trace in Fig. 1 shows evidence of an intermediate plateau at $T\approx550$ °C. This plateau corresponds to an average Mn valence of *ca.* +3 and was observed for all compositions

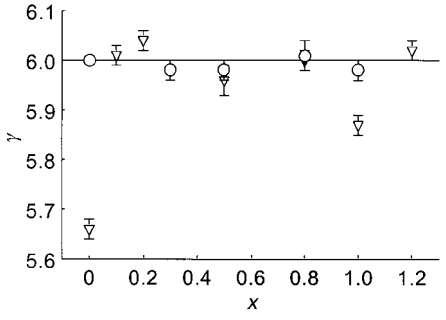

Fig. 2 Oxygen content, γ, in as-prepared samples (▽) and in samples annealed in oxygen for 16 h at 800 °C and $p(O_2)\approx100$ atm (○).

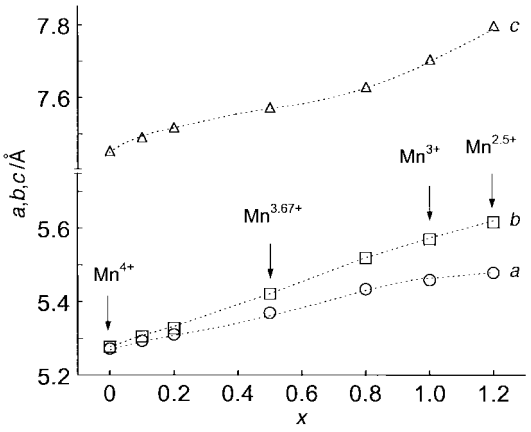

Fig. 3 Orthorhombic unit cell parameters for $Ca_2Mn_{2-x}Nb_xO_{6.0}$: variation with x.

$x\leqslant0.8$. It possibly indicates a significant stabilisation of the intermediate Mn^{3+} state during reduction.

The powder XRD data for all fully oxidised samples were indexed on a similar orthorhombic unit cell to that of Ca_2MnNbO_6, which has a basic $\sqrt{2}\times\sqrt{2}\times2$ relation to the cubic perovskite subcell but superposed on which are small variations in lattice parameters associated with orthorhombic distortions. The unit cell parameters and cell volume are plotted against x in Fig. 3 and 4; in spite of a linear variation in V, the individual parameters show markedly non-linear variation, indicating varying degrees of structural distortion, perhaps associated with the changing oxidation state of Mn.

XRD data of the fully reduced materials showed single phase products for the two end-members and a mixture of the reduced end-members for intermediate compositions. For $Ca_2Mn_{0.8}Nb_{1.2}O_\gamma$, the XRD pattern of the reduced material $\gamma=5.80$ was similar to that of $\gamma=6.00$, but with slightly increased cell dimensions. It is concluded that this reduced composition corresponds to single phase $Ca_2Mn^{2+}{}_{0.8}Nb_{1.2}O_{5.8}$.

For $CaMnO_{3-\delta}$, the product of reduction had a simple cubic pattern, similar to those of CaO and MnO but with intermediate *d*-spacings. This phase appears to have a rock salt structure therefore, with Ca^{2+} and Mn^{2+} ions disordered over the octahedral sites of the face centred cubic unit cell. Unit cell data for CaO, MnO and three intermediate compositions[18–20] are plotted against composition in Fig. 5. A linear dependence is obtained, showing Vegard's law behaviour. The unit cell data for the fully reduced phase, (Ca,Mn)O, $a=$ 4.630 Å, gave a composition, by interpolation in Fig. 5, that corresponded very closely to the expected composition $Ca_{0.5}Mn_{0.5}O$.

For all intermediate compositions x in the $Ca_2Mn_{2-x}Nb_xO_\gamma$ solid solutions, the products of complete reduction were identified by XRD to be mixtures of (Ca,Mn)O and

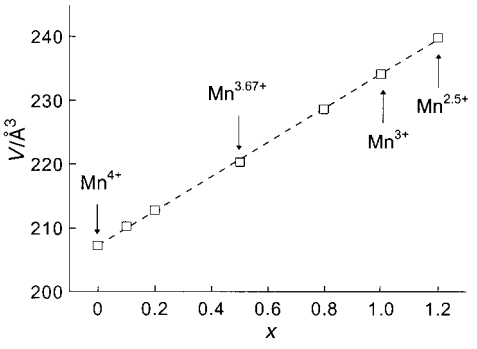

Fig. 4 Volume of orthorhombic unit cell in $Ca_2Mn_{2-x}Nb_xO_{6.0}$: variation with x.

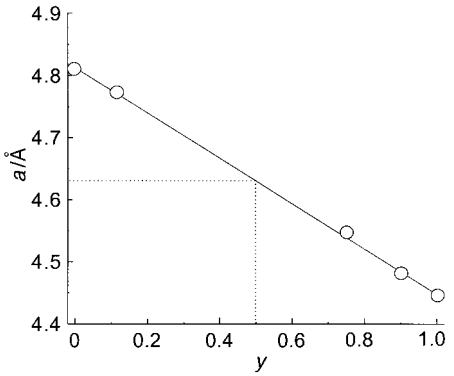

Fig. 5 Variation of unit cell parameter, a, in solid solution $Ca_{1-y}Mn_yO$.

$Ca_2Mn_{0.8}Nb_{1.2}O_{5.8}$. In order to investigate the products of partial reduction of the solid solutions, and particularly, investigate the range of γ values over which single phase solid solutions could exist prior to decomposition, a series of H_2 reduction TG experiments were carried out in which the experiments were terminated at various stages of reduction. Samples were cooled in the TG apparatus thus allowing the final oxygen contents to be determined and the products analysed by XRD.

Two types of behaviour were observed on partial reduction. First, all compositions showed that some oxygen could be removed whilst retaining the original structure; however, unit cells expanded and orthorhombicity generally decreased on decreasing γ. Typically, γ could be reduced to 5.7 ± 0.1 whilst retaining an orthorhombic structure.

Second, compositions in the range $x=0.30$–0.80 gradually transformed, through decreasing orthorhombicity, into simple cubic structures that had perovskite-like XRD patterns (Table 1). The variation in cell volume for one composition, $x=0.50$, is shown in Fig. 6; a linear plot is obtained for the combined orthorhombic ($\gamma\geqslant5.8$) and cubic ($\gamma\leqslant5.5$) structure. For $\gamma\leqslant5.1$, the cubic structure decomposed into a mixture of the reduced end-members, (Ca,Mn)O and $Ca_2Mn_{0.8}Nb_{1.2}O_{5.8}$.

Table 1 X-ray powder diffraction data for $Ca_2Mn_{1.5}Nb_{0.5}O_{5.47(2)}$ cubic: $a=3.8265(4)$ Å

$h\ k\ l$	I	d(obs)/Å	d(calc)/Å
1 0 0	20	3.8327	3.8265
1 1 0	100	2.7067	2.7057
2 0 0	54	1.9129	1.9132
2 1 0	13	1.7104	1.7113
2 1 1	45	1.5618	1.5622
2 2 0	14	1.3528	1.3529
2 2 1, 3 0 0	5	1.2756	1.2755
3 1 0	9	1.2102	1.2100

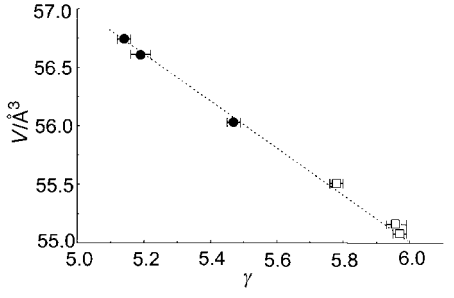

Fig. 6 Variation of (□) reduced orthorhombic unit cell volume, 1/4 V_{or}, and (●) cubic unit cell volume, V_c, with oxygen content in $Ca_2Mn_{1.5}Nb_{0.5}O_\gamma$.

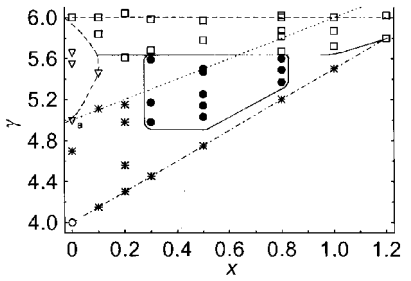

Fig. 7 Phase diagram of $Ca_2Mn_{2-x}Nb_xO_\gamma$ solid solution: (□) orthorhombic perovskite, (●) cubic perovskite, (▽) perovskite-related phase with ordering of oxygen vacancies, (○) rock salt (Ca,Mn)O, (∗) phase mixture of rock salt (Ca,Mn)O and perovskite, (a) literature value;[21] (–––––) $\gamma=6.00$, (-----) Mn^{3+}, (–·––) Mn^{2+}.

The phase diagram $Ca_2Mn_{2-x}Nb_xO_\gamma$

The results of post-reaction heat treatments in both air and H_2–N_2 have been combined into a phase diagram showing the compositional stability fields of the different solid solution structure types (Fig. 7). This is not an equilibrium phase diagram in which solid solution compositions are shown as a function of, for example, temperature or oxygen partial pressure, but instead shows the maximum range of solid solution compositions that can be achieved by varying the conditions of synthesis. Three single phase areas are identified. First, the orthorhombic solid solutions cover the entire range of x values and with varying degrees of partial reduction to give typically $5.6<\gamma<6.0$. Second, a range of cubic solid solutions with $0.3\leqslant x\leqslant0.8$ and $(5.0$–$5.3)\leqslant\gamma\leqslant5.6$. Third, reduced $CaMnO_3$, for which superstructure lines are seen by powder XRD and various intergrowth structures have been seen by electron microscopy:[1] similar superstructure lines were found for solid solutions with low x values, *e.g.* composition $x=0.1$. The remaining regions of the phase diagram (Fig. 7) correspond to mixtures of phases.

Also superposed on Fig. 7 are lines corresponding to average Mn oxidation states (determined from the γ values) of $+2$ and $+3$. It can be seen that depending on x, the orthorhombic solid solutions have Mn oxidation states covering the complete range between $+2$ and $+4$ whereas the cubic solid solutions are largely confined to the range $+2$ to $+3$.

The increase in unit cell volume with decreasing γ, and therefore decreasing average oxidation state of Mn, is shown for one composition x in Fig. 6. In Fig. 8, the unit cell volume is shown with a constant Mn oxidation state of $+3$ but with varying x and γ. Perhaps surprisingly, the cell volume *decreases* as oxygen is removed from the structure and the average B cation oxidation state decreases.

Variation of oxygen content γ with temperature and composition x in air

In order to determine the equilibrium oxygen contents at $p(O_2)=0.21$ as a function of T and x, heat/cool TG traces in

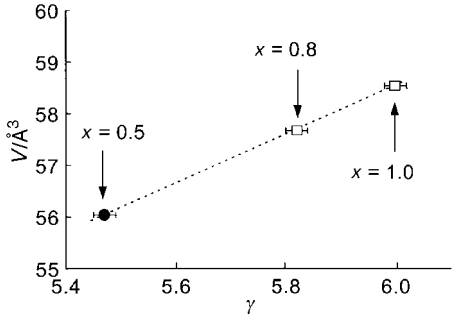

Fig. 8 Unit cell volume of solid solution, $Ca_2Mn^{3+}{}_{2-x}Nb_xO_\gamma$: variation with γ; (●) cubic and (□) orthorhombic phases.

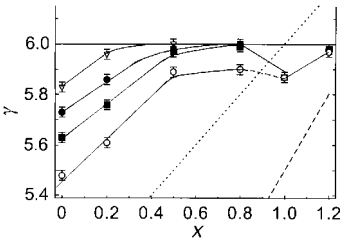

Fig. 9 Equilibrium oxygen contents of the $Ca_2Mn_{2-x}Nb_xO_\gamma$ series at high temperatures in air: (▽) 1000 °C, (●) 1100 °C, (■) 1200 °C, (○) 1350 °C; (-----) Mn^{3+}, (–––––) Mn^{2+}.

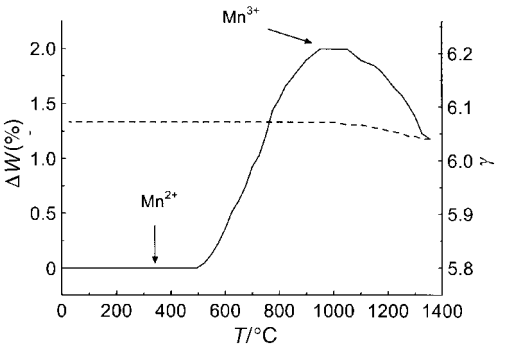

Fig. 10 Weight change of $Ca_2Mn_{0.8}Nb_{1.2}O_{5.8}$ during heating (———) and cooling (– – – – –) in air.

air were recorded for samples that had been previously fully oxygenated, with $\gamma = 6.0$. For the temperature ranges over which the TG data were fully reversible, the equilibrium values of γ in air could be determined, thus providing useful practical information on the variation of γ with heat treatments in air. The TG results may be summarised as follows: $x = 0$: complete reversibility for $5.5 < \gamma < 6.0$ over the temperature range $1350 > T > 850$ °C; $x = 0.2$: almost complete reversibility $5.6 < \gamma < 6.0$ over the range $1350 > T > 950$ °C; $x = 0.5$: approximate reversibility over the ranges $5.89 < \gamma < 5.98$ and $1350 > T > 1150$ °C; $x = 0.8$: approximate reversibility over the ranges $5.90 < \gamma < 6.0$ and $1350 > T > 1050$ °C; $x = 1.0$: constant $\gamma \approx 5.87$ at $T > 1100$ °C. (Previous investigations showed a small variation of γ at low temperatures with $\gamma \approx 5.94$ at $T < 500$ °C and $\gamma \approx 5.87$ at $T > 700$ °C;[9]) $x = 1.2$: approximate reversibility over the ranges $5.97 < \gamma < 6.01$ at $1350 > T > 1100$ °C.

These results were used to construct the equilibrium phase diagram shown in Fig. 9, in which the oxygen content, in air, is given for temperatures in the range 1000–1350 °C. The oxygen content shows greatest variation at low x (0, 0.2), limited variation at intermediate x (0.5, 0.8) and little or no variation at high x ($\geqslant 1.0$). Almost all the data are for the orthorhombic solid solution with the $GdFeO_3$ structure. Thus, the cubic, heavily oxygen-deficient solid solutions may appear on an equilibrium phase diagram at lower partial pressures or they may exist only as metastable solid solutions that are produced by low temperature H_2 reduction. Similarly, the thermodynamic status of oxygen-stoichiometric Ca_2MnNbO_6 is not known since high pressure oxidation at low temperatures (*ca.* 600 °C) is required to achieve this stoichiometry.

Synthesis of oxygen-excess, $Ca_2Mn_{0.8}Nb_{1.2}O_{6.2}$

For all the studies described so far, the maximum oxygen content achievable was $\gamma = 6.0$ and XRD data of samples that had been reduced and subsequently reoxidised showed complete reversibility. The one exception to this pattern of behaviour occurred with composition $x = 1.2$. In the as-prepared condition, its formula may be given as $Ca_2Mn_{0.8}{}^{2.5+}Nb_{1.2}O_{6.0}$. After H_2-reduction, it changed to $Ca_2Mn_{0.8}{}^{2+}Nb_{1.2}O_{5.8}$. On subsequent reoxidation at low temperatures however, it picked up extra oxygen, to give the formula $Ca_2Mn_{0.8}{}^{3+}Nb_{1.2}O_{6.2}$ as shown by TG (Fig. 10). The resulting material, which formed over the range *ca.* 750–1000 °C, subsequently lost oxygen at higher temperatures, to return to an oxygen content close to 6.0. XRD data for compositions with $\gamma = 5.8$, 6.0 and 6.2 are shown in Fig. 11. Data for $\gamma = 5.8$ and 6.0 are very similar, with small differences in *d*-spacings and peak splittings characteristic of the $GdFeO_3$ distortion of the perovskite structure. The XRD data for $\gamma = 6.2$ show single broad, asymmetric peaks instead of the peak multiplets seen for $x = 5.8$ and 6.0. Clearly the oxidation process has reduced the crystalline quality and probably the particle size.

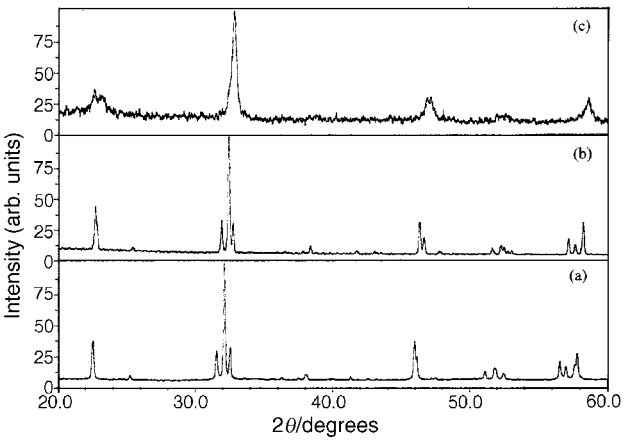

Fig. 11 XRD patterns for compositions $Ca_2Mn_{0.8}Nb_{1.2}O_\gamma$ with (a) $\gamma = 5.8$, (b) $\gamma = 6.0$ and (c) $\gamma = 6.2$.

Discussion

The $Ca_2Mn_{2-x}Nb_xO_\gamma$ solid solutions are compositionally complex since they exist over a wide range of x and γ values. Both ionic and electronic mechanisms of charge balance occur. Thus, although crystallographic data are required to confirm this, the structures appear to be able to tolerate up to *ca.* 20% of vacancies in the oxygen sublattice in samples that have been either heated in air to high temperatures or partially reduced in H_2. In addition, the Mn oxidation state can have any (average) value between +2 and +4, again dependent on sample processing conditions.

As well as their compositional complexity, the structures of the solid solutions are variable. Solid solutions with the entire range of cation contents, and zero or small deficiencies in oxygen content, appear to have the orthorhombic $GdFeO_3$ structure. With larger degrees of reduction and oxygen deficiency, a range of cation contents shows an apparently simple, cubic perovskite structure.

The oxygen content of most compositions can be varied by heating in air at different temperatures above *ca.* 800 °C. The variation is greatest, and the rates of O_2 desorption/uptake most rapid for $CaMnO_3$ ($x = 0$) and generally decrease with x. For $x = 1$, the oxygen content varies little on heating in air but does vary on H_2 reduction or heating in O_2 at high pressures. This composition, $x = 1$, is anomalous in that, in order to achieve an oxygen content of $\gamma = 6.0$, heating in O_2 at high pressures is needed. As speculated previously, this may reflect the structural constraints imposed upon Mn^{3+} by the surrounding Ca–Nb–O framework which does not permit the Mn^{3+} ion to occupy grossly distorted octahedra and thereby to exhibit its intrinsic Jahn–Teller effect.

One composition, $Ca_2Mn_{0.8}Nb_{1.2}O_{6.2}$, was prepared with an oxygen content in excess of 6.0. The driving force for this is

believed to be the complete oxidation of Mn^{2+} to Mn^{3+}. However, since the perovskite (or $GdFeO_3$) structure cannot accommodate interstitial oxygens, the structure must instead have cation vacancies (both A and B sites) within a full oxygen sublattice. The large amount of cation diffusion required results in a major disruption in the crystal structure of the $Ca_2Mn_{0.8}Nb_{1.2}O_\gamma$ parent phase, as shown by a decrease in crystallinity from its XRD pattern and the possible precipitation of small amounts of $Ca_2Nb_2O_7$.

Work is in progress to measure magnetic and electrical properties of the solid solutions as a function of composition; this will be reported subsequently.

References

1 A. Reller, J. M. Thomas, D. A. Jefferson and M. K. Uppal, *Proc. R. Soc. London*, *A*, 1984, **394**, 447.
2 Y. Takeda, R. Kanno, T. Takada, O. Yamamoto, M. Takano and Y. Bando, *Z. Anorg. Allg. Chem.*, 1986, **540–541**, 259.
3 Y. Takeda, R. Kanno, T. Takada, O. Yamamoto, M. Takano, N. Nakayama and Y. Bando, *J. Solid State Chem.*, 1986, **63**, 237.
4 A. Nemudry, P. Rudolf and R. Schöllhorn, *Chem. Mater.*, 1996, **8**, 2232.
5 J. C. Grenier, S. Ghodbane, G. Demazeau, M. Pouchard and P. Hagenmuller, *Mater. Res. Bull.*, 1979, **14**, 831.
6 J. Berggren, *Acta Chem. Scand.*, 1971, **25**, 3616.
7 J. A. Chavez, T. C. Gibb and A. R. West, *J. Mater. Chem.*, 1996, **6**, 1957.
8 P. Hagenmuller, M. Pouchard and J. C. Grenier, *Solid State Ionics*, 1990, **43**, 7.
9 A. Kruth, PhD Thesis, University of Aberdeen, 1999.
10 A. Kruth, M. Tabuchi, U. Guth and A. R. West, *J. Mater. Chem.*, 1998, **8**, 11.
11 R. Rodríguez, A. Fernández, A. Isalgué, J. Rodríguez, A. Labarta, J. Tejada and X. Obradors, *J. Solid State Phys.*, 1985, **18**, L401.
12 T. C. Gibb, P. D. Battle, S. K. Bollen and R. J. Whitehead, *J. Mater. Chem.*, 1992, **,** 111.
13 T. C. Gibb, *J. Mater. Chem.*, 1993, **3**, 441.
14 T. C. Gibb, A. J. Herod and N. Peng, *J. Mater. Chem.*, 1995, **5**, 91.
15 P. D. Battle, T. C. Gibb, A. J. Herod, S.-H. Kim and P. H. Munns, *J. Mater. Chem.*, 1995, **5**, 865.
16 International Centre for Diffraction Data, card no. 45–1266.
17 International Centre for Diffraction Data, card no. 18–301.
18 International Centre for Diffraction Data, card no. 28–775.
19 International Centre for Diffraction Data, card no. 7–230.
20 International Centre for Diffraction Data, card no. 36–1378.
21 K. R. Poeppelmeier, M. E. Leonowicz, J. C. Scalon and J. M. Longo, *J. Solid State Chem.*, 1982, **45**, 71.

Paper 9/02234A